

Watermark-based Attribution of AI-Generated Content

Zhengyuan Jiang, Moyang Guo, Yuepeng Hu, Neil Zhenqiang Gong
Duke University
{zhengyuan.jiang, moyang.guo, yuepeng.hu, neil.gong}@duke.edu

ABSTRACT

Several companies have deployed watermark-based detection to identify AI-generated content. However, attribution—the ability to trace back to the user of a generative AI (GenAI) service who created a given piece of AI-generated content—remains largely unexplored despite its growing importance. In this work, we aim to bridge this gap by conducting the first systematic study on watermark-based, user-level attribution of AI-generated content. Our key idea is to assign a unique watermark to each user of the GenAI service and embed this watermark into the AI-generated content created by that user. Attribution is then performed by identifying the user whose watermark best matches the one extracted from the given content. This approach, however, faces a key challenge: How should watermarks be selected for users to maximize attribution performance? To address the challenge, we first theoretically derive lower bounds on detection and attribution performance through rigorous probabilistic analysis for any given set of user watermarks. Then, we select watermarks for users to maximize these lower bounds, thereby optimizing detection and attribution performance. Our theoretical and empirical results show that watermark-based attribution inherits both the accuracy and (non-)robustness properties of the underlying watermark. Specifically, attribution remains highly accurate when the watermarked AI-generated content is either not post-processed or subjected to common post-processing such as JPEG compression, as well as black-box adversarial post-processing with limited query budgets.

1 Introduction

Generative AI (GenAI)—such as DALL-E, Midjourney, and ChatGPT—can produce highly realistic content in various forms, such as images, text, and audio. While GenAI offers numerous societal benefits, it also raises significant ethical concerns. For example, it can be misused to create harmful content, support disinformation and propaganda campaigns by generating realistic-looking fake material [1], and enable individuals to falsely claim copyright ownership of AI-generated content [2].

Watermark-based detection of AI-generated content has emerged as a promising technique to address these ethical concerns. Specifically, existing work on watermark-based detection primarily focuses on two lines of research. The first aims to develop watermarks that are robust against post-processing. Notably, while creating fully robust watermarks remains an ongoing challenge, the field has made significant progress in recent years. For example, non-learning-based image watermarks [3–5], which have been studied for decades, are generally not robust to common post-processing such as JPEG compression, Gaussian blur, and brightness/contrast adjustments. However, recent advancements in learning-based image watermarks [6–12] have shown robust performance against common post-processing. Notably, some learning-based watermarks [12] are even certifiably robust, ensuring resilience against any post-processing that introduces bounded perturbations to the images. While these watermarks are not yet robust against strong adversarial post-processing in white-box settings [13], they demonstrate strong robustness in black-box scenarios [13].

The second line of research leverages watermarks as a proactive strategy to detect AI-generated content. Specifically, a watermark is embedded into all content generated by a GenAI service, and a piece of content is identified as AI-generated if a similar watermark can be decoded from it. Due to its potential, watermark-based detection has garnered significant attention. For instance, the Executive Order issued by the White House in October 2023 recommended watermarking AI-generated content. Several major companies have already deployed watermark-based detection. For example, OpenAI embeds visible watermarks into images generated by DALL-E [14], while Google’s SynthID [15]

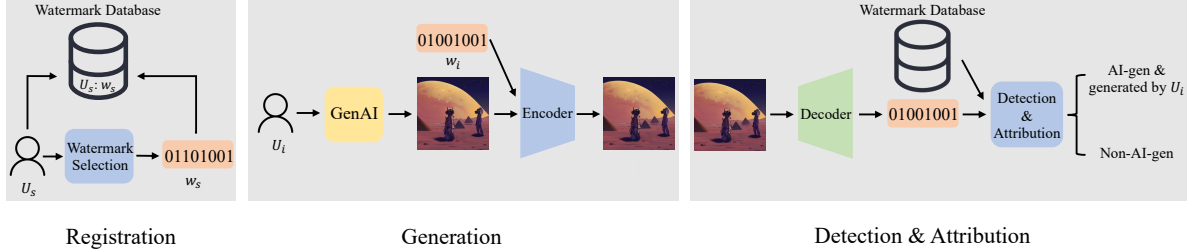


Figure 1: *Registration, generation, and detection & attribution* phases of watermark-based detection and attribution.

uses invisible watermarks in images produced by its Imagen. Stability AI deploys watermarks in Stable Diffusion [16], and Microsoft watermarks all AI-generated images created via Bing [17].

Attribution seeks to trace the origin of a piece of content detected as AI-generated, specifically identifying the user of the GenAI service who created it.¹ This capability is crucial for aiding GenAI service providers and law enforcement in forensic investigations of cybercrimes, such as disinformation and propaganda campaigns involving AI-generated content. Despite its increasing importance, attribution remains largely unexplored.

Our work: In this work, we bridge this gap by conducting the *first* systematic study on watermark-based, user-level attribution of AI-generated content. Figure 1 illustrates our core idea. When a user registers with a GenAI service, the service provider assigns the user a unique watermark (i.e., a bitstring) and stores it in a watermark database. Whenever the user generates content using the GenAI service, their specific watermark is embedded in the content. A piece of content is attributed to the user whose watermark is the most similar to the one extracted from the content. Our approach differs from standard user-agnostic watermark-based detection, where the same watermark is embedded in all AI-generated content. Thus, our approach also introduces a slight modification in the detection process: content is identified as generated by the GenAI service if the extracted watermark closely matches *at least* one user’s watermark.

However, our approach faces a significant challenge: how should watermarks be selected for users to maximize detection and attribution performance? A straightforward solution is to empirically evaluate the detection and attribution performance for different numbers of users and corresponding watermark sets. However, this method is difficult to scale due to the vast space of possible watermarks. For instance, a 64-bit watermark yields 2^{64} potential watermarks, resulting in $\binom{2^{64}}{s}$ possible watermark sets for s users. Evaluating the detection and attribution performance for each watermark set to find the optimal one is computationally infeasible.

We propose a two-step solution to address this challenge. First, we conduct a rigorous probabilistic analysis to theoretically evaluate user-aware detection and attribution performance for *any* given set of user watermarks. Specifically, we formally quantify the behavior of watermarking and derive lower bounds for the *true detection rate (TDR)* and *true attribution rate (TAR)*, as well as an upper bound for the *false detection rate (FDR)*. TDR (or TAR) represents the probability of correctly detecting (or attributing) AI-generated content, while FDR denotes the probability of incorrectly classifying non-AI-generated content as AI-generated. We also show that other relevant performance metrics can be derived from these three core metrics.

In the second step of our solution, we select watermarks for users to maximize the lower bounds of TDR and TAR, thereby optimizing TDR and TAR. Based on the analytical forms of these lower bounds, this optimization simplifies to selecting the most dissimilar watermarks for users. Formally, we define the *watermark selection problem*, which seeks to assign a watermark to a new user by minimizing the maximum similarity between the new watermark and those of existing users. We find that this problem is equivalent to the well-known *farthest string problem* [18], extensively studied in theoretical computer science. However, since the farthest string problem is NP-hard, our watermark selection problem is also NP-hard, posing significant challenges in developing efficient *exact* solutions. Consequently, we focus on efficient *approximate* solutions. Specifically, we adapt the *bounded search tree algorithm* [19], a state-of-the-art, albeit inefficient, exact solution for the farthest string problem, into an efficient approximate algorithm for watermark selection.

We empirically evaluate our method on non-AI-generated images from three standard image benchmark datasets and AI-generated images produced by three GenAI models: Stable Diffusion, Midjourney, and DALL-E. For watermarking, we use HiDDeN [7], which is the basis for modern learning-based watermarking technique. Our results show that detection and attribution are highly accurate, with TDR and TAR close to 1 and FDR near 0, when AI-generated images

¹Attribution can also refer to identifying the GenAI service responsible for generating the content, as discussed in Section 8.

are not post-processed, even for GenAI services with a large user base (e.g., 100 million users). Performance remains high under common post-processing operations such as JPEG compression, Gaussian blur, and brightness/contrast adjustments. Additionally, adversarial post-processing [13] with a limited number of queries to the detection API significantly degrades image quality to evade detection and attribution. Furthermore, our watermark selection algorithm outperforms baseline methods, and we show that our approach is also applicable to AI-generated text.

To summarize, our contributions are as follows:

- We conduct the *first* systematic study on watermark-based, user-level attribution of AI-generated content.
- We formally quantify the behavior of watermarking, based on which we provide a theoretical analysis of detection and attribution performance for any given set of user watermarks.
- Building on our theoretical insights, we formulate watermark selection as an optimization problem and develop an efficient approximate solution.
- We evaluate our method across various scenarios.

2 Related Work on Watermarks

A watermarking method typically consists of three components: *watermark*, *encoder*, and *decoder*. We consider a watermark w to be a bitstring. An encoder E embeds a watermark into content, while a decoder D decodes a watermark from a (watermarked or unwatermarked) content. When a content has watermark w , the decoded watermark is similar to w . The encoder E and watermark w can also be embedded into the parameters of a GenAI model such that its generated content is inherently watermarked with w [10].

Non-learning-based vs. learning-based: Watermarking methods can be categorized into two groups based on the design of the encoder and decoder: *non-learning-based* and *learning-based*. Non-learning-based methods [3–5, 20, 21] design the encoder and decoder based on some hand-crafted heuristics, while learning-based methods [6–10, 12, 22, 23] use neural networks as the encoder/decoder and automatically learn them using a content dataset. For instance, Tree-Ring [20] and LM-watermarking [21] respectively are non-learning-based watermarking methods for images and texts; while HiDDeN [7] and AWT [22] respectively are learning-based methods for images and texts. Our theoretical analysis and watermark selection algorithm are applicable to both categories of watermarking methods as long as they use bitstring-based watermarks such as HiDDeN [7], Stable Signature [10], StegaStamp [23], and Smoothed HiDDeN/StegaStamp [12]. Since learning-based methods are more robust due to adversarial training [7], we adopt a learning-based method in our experiments. In particular, we use HiDDeN, which is the basis for modern learning-based watermarking methods.

Standard training vs. adversarial training: In learning-based watermarking methods, the encoder and decoder are automatically learnt using a content dataset. Specifically, given a content C and a random watermark w , the decoded watermark $D(E(C, w))$ for the watermarked content $E(C, w)$ should be similar to w , i.e., $D(E(C, w)) \approx w$. Based on this intuition, *standard training* aims to learn an encoder E and decoder D such that $D(E(C, w))$ is similar to w for a content dataset [6]. A watermarked content $E(C, w)$ may be post-processed, e.g., a watermarked image may be post-processed by JPEG compression during transmission on the Internet. Zhu et al. [7] extended adversarial training [24, 25], a standard technique to train robust classifiers, to train watermarking encoder and decoder that are more robust against post-processing. Specifically, *adversarial training* aims to learn an encoder E and decoder D such that $D(P(E(C, w)))$ is similar to w , where P stands for a post-processing operation and $P(E(C, w))$ is a post-processed watermarked content. In each epoch of adversarial training, a P is randomly sampled from a given set of them for each content in the content dataset.

Robustness of watermarking: We stress that building robust watermarking methods is *orthogonal* to our work that leverages an existing watermarking method for user-level attribution of AI-generated content. Non-learning-based watermarking methods [3–5, 20, 21] are known to be non-robust to *common post-processing* such as JPEG compression for images [7, 10] and paraphrasing for texts [26], i.e., such common post-processing can remove the watermark from a watermarked content. Learning-based watermarking methods [6–10, 22] are more robust to such common post-processing because they can leverage adversarial training. For instance, common post-processing has to substantially decrease the quality of a watermarked image in order to remove the watermark [8, 9].

Adversarial post-processing [13, 27] strategically perturbs a watermarked image to remove the watermark. Learning-based image watermarking methods are not yet robust to adversarial post-processing in the white-box setting where an attacker has access to the decoder. However, they have good robustness to adversarial post-processing when an attacker can only query the detection API for a small number of times in the black-box setting [12] or the attacker has

limited computation resource to train a small number of surrogate watermarking models in transfer attacks [28]. In particular, adversarial post-processing substantially decreases the quality of a watermarked image in order to remove the watermark in such scenarios. To enhance robustness, a GenAI service can keep its watermarking encoder/decoder private and restrict the API access to a small number of trusted customers. For instance, Google’s SynthID [15] adopts such strategy.

3 Problem Formulation

Problem setup: Suppose a GenAI model is deployed as a GenAI cloud service. A registered user sends a *prompt* (i.e., a text) to the GenAI service, which returns an AI-generated content to the user. The content can be image, text, or audio. *Detection* of AI-generated content aims to decide whether a given content was generated by the GenAI service or not; while *attribution* further traces back the user of the GenAI service who generated a content detected as AI-generated. Such attribution can aid the GenAI service provider or law enforcement in forensic investigations of cyber-crimes, e.g., disinformation or propaganda campaigns, that involve AI-generated content. We formally define the detection and attribution problems as follows:

Definition 1 (Detection of AI-generated content). *Given a content and a GenAI service, detection aims to infer whether the content was generated by the GenAI service or not.*

Definition 2 (Attribution of AI-generated content). *Given a content, a GenAI service, and s users $U = \{U_1, U_2, \dots, U_s\}$ of the GenAI service, attribution aims to further infer which user used the GenAI service to generate the content after it is detected as AI-generated.*

We note that the set of s users U in attribution could include all registered users of the GenAI service, in which s may be very large. Alternatively, this set may consist of a smaller number of registered users if the GenAI service provider has some prior knowledge on its registered users. For instance, the GenAI service provider may exclude the registered users, who are verified offline as trusted, from the set U to reduce its size. Moreover, malicious users may be identified by conventional network security solutions, such as IP addresses and behavior patterns [29–31]. How to construct the set of users U in attribution is out of the scope of this work. Given any set U , our method aims to infer which user in U may have generated a given content. We also note that another relevant attribution problem is to trace back the GenAI service that generated a given content. Our method can also be used for such GenAI-service attribution, which we discuss in Section 8.

Threat model: An AI-generated, watermarked content may be post-processed by some *common post-processing* techniques in *non-adversarial settings*. For instance, an image may be post-processed by JPEG compression during transmission on the Internet, or a user may use Gaussian blur or Brightness/Contrast to edit an image in an image editor. In *adversarial settings*, a malicious user may post-process an AI-generated content to evade detection and/or attribution. Other than the common post-processing techniques, a malicious user may also use *adversarial post-processing* [13] to remove the watermark in an AI-generated content. We assume the watermark encoder/decoder is private and the malicious user has limited access to the detection API, in which state-of-the-art watermarking methods have good robustness to post-processing [13]. Such threat model arises when a GenAI service provider restricts the access of its detection API to a small set of trusted customers, e.g., Google’s SynthID adopts this threat model. Note that our theoretical analysis in Section 5 can explicitly quantify and incorporate the impact of post-processing on the detection and attribution performance.

4 Watermark-based Attribution

4.1 Overview

Figure 1 illustrates our watermark-based detection and attribution of AI-generated content. When a user registers in the GenAI service, the service provider selects a unique watermark for the user. We denote by w_i the watermark selected for user U_i , where i is the user index. During content generation, when a user U_i sends a prompt to the GenAI service to generate a content, the provider uses the watermark encoder E to embed watermark w_i into the content. Since our method differs from standard user-agnostic watermark-based detection, where the same watermark is embedded in all AI-generated content, our method also introduces a slight modification in the detection process: a given content is identified as generated by the GenAI service if the extracted watermark closely matches at least one user’s watermark. Furthermore, during attribution, the given content is attributed to the user whose watermark is the most similar to the decoded watermark. Next, we describe the details of detection and attribution.

4.2 Detection

Recall that we denote by $U = \{U_1, U_2, \dots, U_s\}$ the set of s users of the GenAI service. Each user U_i has a watermark w_i , where $i = 1, 2, \dots, s$. For convenience, we denote by $W = \{w_1, w_2, \dots, w_s\}$ the set of s watermarks. Given a content C , we use the decoder D to decode a watermark $D(C)$ from it. If there exists a user's watermark that is similar enough to $D(C)$, we detect C as AI-generated. We use *bitwise accuracy* to measure similarity between two watermarks, which we formally define as follows:

Bitwise Accuracy (BA): Given any two watermarks w and w' , their bitwise accuracy (denoted as $BA(w, w')$) is the fraction of matched bits in them. Formally, we have:

$$BA(w, w') = \frac{1}{n} \sum_{k=1}^n \mathbb{I}(w[k] = w'[k]), \quad (1)$$

where n is the watermark length, $w[k]$ is the k th bit of w , and \mathbb{I} is the indicator function that has a value 1 if $w[k] = w'[k]$ and 0 otherwise. A content C is detected as AI-generated if and only if the following satisfies:

$$\max_{i \in \{1, 2, \dots, s\}} BA(D(C), w_i) \geq \tau, \quad (2)$$

where $\tau > 0.5$ is the *detection threshold*.

4.3 Attribution

Attribution is applied only after a content C is detected as AI-generated. Intuitively, we attribute the content to the user whose watermark is the most similar to the decoded watermark $D(C)$. Formally, we attribute content C to user U_{i^*} , where i^* is as follows:

$$i^* = \arg \max_{i \in \{1, 2, \dots, s\}} BA(D(C), w_i). \quad (3)$$

4.4 Key Challenge

Our watermark-based attribution faces a key challenge: how to select watermarks for users to maximize detection and attribution performance. To tackle this, we first perform a rigorous probabilistic analysis to derive lower bounds on detection and attribution performance for any given set of user watermarks. Then, we select user watermarks to maximize these lower bounds, thereby optimizing the detection and attribution performance. Given the analytical forms of these lower bounds, this optimization reduces to selecting the most dissimilar watermarks for users. Thus, we design an efficient algorithm to select user watermarks with maximal dissimilarity. Below, we first present our theoretical analysis of detection and attribution performance, followed by a detailed description of our algorithm to select user watermarks that maximize the detection and attribution performance.

5 Detection and Attribution Performance

We theoretically analyze the detection and attribution performance of our method for *any* given set of user watermarks. To this end, we first formally define three core metrics to evaluate performance: *true detection rate (TDR)*, *true attribution rate (TAR)*, and *false detection rate (FDR)*. We demonstrate that other relevant performance metrics can be derived from these three. Then, we formally quantify the behavior of a watermarking method. Based on this quantification, we derive lower bounds of TDR and TAR, as well as an upper bound of FDR for any given set of user watermarks. All our proofs are shown in Appendix.

5.1 Content Distributions

Suppose we are given s users $U = \{U_1, U_2, \dots, U_s\}$, each of which has a unique watermark w_i , where $i = 1, 2, \dots, s$. We denote the s watermarks as a set $W = \{w_1, w_2, \dots, w_s\}$. When a user U_i generates content via the GenAI service, the service provider uses the encoder E to embed the watermark w_i into the content. We denote by \mathcal{P}_i the probability distribution of the watermarked content generated by U_i . Note that two users U_i and U_j may have different AI-generated, watermarked content distributions \mathcal{P}_i and \mathcal{P}_j . This is because the two users have different watermarks and they may be interested in generating different types of content. Moreover, we denote by \mathcal{Q} the probability distribution of non-AI-generated content.

5.2 Evaluation Metrics

(User-dependent) True Detection Rate (TDR): TDR is the probability that an AI-generated content is correctly detected. Note that different users may have different AI-generated content distributions. Therefore, TDR depends on users. We denote by TDR_i the true detection rate for the watermarked content generated by user U_i , i.e., TDR_i is the probability that a content C sampled from the probability distribution \mathcal{P}_i uniformly at random is correctly detected as AI-generated. Formally, we have:

$$TDR_i = \Pr(\max_{j \in \{1, 2, \dots, s\}} BA(D(C), w_j) \geq \tau), \quad (4)$$

where BA is the bitwise accuracy between two watermarks, D is the decoder, $C \sim \mathcal{P}_i$, and τ is the detection threshold. The notation \sim indicates a content is sampled from a distribution uniformly at random.

False Detection Rate (FDR): FDR is the probability that a content C sampled from the non-AI-generated content distribution \mathcal{Q} uniformly at random is detected as AI-generated. Note that FDR does not depend on users. Formally, we have:

$$FDR = \Pr(\max_{j \in \{1, 2, \dots, s\}} BA(D(C), w_j) \geq \tau), \quad (5)$$

where $C \sim \mathcal{Q}$.

(User-dependent) True Attribution Rate (TAR): TAR is the probability that an AI-generated content is correctly attributed to the user that generated the content. Like TDR, TAR also depends on users. We denote by TAR_i the true attribution rate for the watermarked content generated by user U_i , i.e., TAR_i is the probability that a content sampled from \mathcal{P}_i uniformly at random is correctly attributed to user U_i . Formally, we have:

$$TAR_i = \Pr(\max_{j \in \{1, 2, \dots, s\}} BA(D(C), w_j) \geq \tau \wedge BA(D(C), w_i) > \max_{j \in \{1, 2, \dots, s\} / \{i\}} BA(D(C), w_j)), \quad (6)$$

where $C \sim \mathcal{P}_i$, the first term $\max_{j \in \{1, 2, \dots, s\}} BA(D(C), w_j) \geq \tau$ means that C is detected as AI-generated, and the second term $BA(D(C), w_i) > \max_{j \in \{1, 2, \dots, s\} / \{i\}} BA(D(C), w_j)$ means that C is attributed to user U_i . Note that we have the first term because attribution is only applied after detecting a content as AI-generated.

Other evaluation metrics can be derived from TDR_i, FDR, and TAR_i: We note that there are also other relevant detection and attribution metrics, e.g., the probability that an AI-generated content is incorrectly attributed to a user. We show that other relevant detection and attribution metrics can be derived from TDR_i, FDR, and TAR_i, and thus we focus on these three metrics in our work. Specifically, Figure 2 shows the taxonomy of detection and attribution results for non-AI-generated content and AI-generated content generated by user U_i . In the taxonomy trees, the first-level nodes represent ground-truth labels of content; the second-level nodes represent possible detection results; and the third-level nodes represent possible attribution results (attribution is performed only after a content is detected as AI-generated).

In the taxonomy trees, there are 5 branches in total, which are labeled as ①, ②, ③, ④, and ⑤ in the figure. Each branch starts from a root node and ends at a leaf node, and corresponds to a metric that may be of interest. For instance, our TDR_i is the probability that a content $C \sim \mathcal{P}_i$ goes through branches ④ or ⑤; FDR is the probability that a content $C \sim \mathcal{Q}$ goes through branch ②; and TAR_i is the probability that a content $C \sim \mathcal{P}_i$ goes through branch ④. The probability that a content goes through other branches can be calculated using TDR_i, FDR, and/or TAR_i. For instance, the probability that a non-AI-generated content $C \sim \mathcal{Q}$ is correctly detected as non-AI-generated is the probability that C goes through the branch ①, which can be calculated as $1 - \text{FDR}$. The probability that an AI-generated content $C \sim \mathcal{P}_i$ is incorrectly detected as non-AI-generated is the probability that C goes through the branch ③, which can be calculated as $1 - \text{TDR}_i$. The probability that a user U_i 's AI-generated content $C \sim \mathcal{P}_i$ is correctly detected as AI-generated but incorrectly attributed to a different user U_j is the probability that C goes through the branch ⑤, which can be calculated as $\text{TDR}_i - \text{TAR}_i$.

5.3 Formal Quantification of Watermarking

Intuitively, to theoretically analyze the detection and attribution performance (i.e., TDR_i, FDR, and TAR_i), we need a formal quantification of a watermarking method's behavior at decoding watermarks in AI-generated content and non-AI-generated content. Towards this end, we formally define β -accurate and γ -random watermarking as follows:

Definition 3 (β -accurate watermarking). *For a randomly sampled AI-generated content $C \sim \mathcal{P}$ embedded with watermark w , the bits of the decoded watermark $D(C)$ are independent and each bit matches with that of w with probability β . Formally, we have $\Pr(D(C)[k] = w[k]) = \beta$, where $C \sim \mathcal{P}$, D is the decoder, and $[k]$ represents the k th bit of a watermark. We say a watermarking method is β -accurate if it satisfies the above condition.*

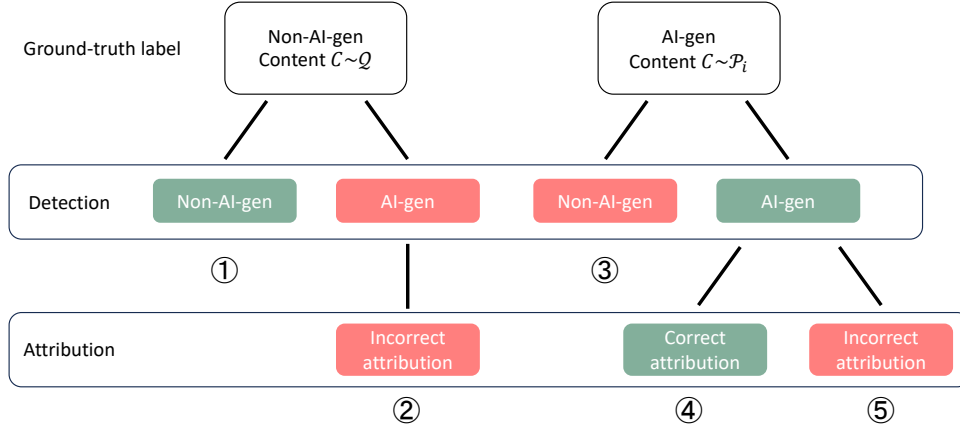


Figure 2: Taxonomy of detection and attribution results. Nodes with red color indicate incorrect detection/attribution.

Definition 4 (γ -random watermarking). *For a randomly sampled non-AI-generated content $C \sim \mathcal{Q}$ without any watermark embedded, the bits of the decoded watermark $D(C)$ are independent and each bit is 1 with probability at least $0.5 - \gamma$ and at most $0.5 + \gamma$, where $\gamma \in [0, 0.5]$. Formally, we have $|\Pr(D(C)[k] = 1) - 0.5| \leq \gamma$, where $C \sim \mathcal{Q}$ and $[k]$ represents the k th bit of a watermark. We say a watermarking method is γ -random if it satisfies the above condition.*

The parameter β is used to characterize the accuracy of the watermarking method at encoding/decoding a watermark in an AI-generated content. In particular, the watermarking method is more accurate when β is closer to 1. For a β -accurate watermarking method, the number of matched bits between the decoded watermark $D(C)$ for a watermarked content C and the ground-truth watermark follows a binomial distribution with parameters n and β , where n is the watermark length. The parameter γ characterizes the behavior of the watermarking method for non-AI-generated content. In particular, the decoded watermark for a non-AI-generated (i.e., unwatermarked) content is close to a uniformly random watermark, where γ quantifies the difference between them. The watermarking method is more random for non-AI-generated content if γ is closer to 0.

User-dependent β_i : Since the users' AI-generated content may have different distributions \mathcal{P}_i , the same watermarking method may have different β for different users. To capture this phenomena, we consider the watermarking method is β_i -accurate for user U_i 's AI-generated content embedded with watermark w_i . Note that the same γ is used across different users since it is used to characterize the behavior of the watermarking method for non-AI-generated content, which is user-independent. The parameters β_i and γ can be estimated using a set of AI-generated and non-AI-generated content, as shown in our experiments.

Incorporating post-processing: Our definition of β -accurate and γ -random watermarking can also incorporate post-processing (e.g., JPEG compression) that an attacker/user may apply to AI-generated or non-AI-generated content. In particular, we can replace $D(C)$ as $D(P(C))$ in our definitions, where P stands for post-processing of content C . When AI-generated content is post-processed, the watermarking method may become less accurate, i.e., β may decrease.

5.4 Detection Performance

Deriving a lower bound of TDR_i : Intuitively, an user U_i 's AI-generated content $C \sim \mathcal{P}_i$ can be correctly detected as AI-generated in two cases:

- **Case I.** The decoded watermark $D(C)$ is similar enough to the user U_i 's watermark w_i .
- **Case II.** The decoded watermark $D(C)$ is dissimilar to w_i but similar enough to some other user's watermark.

Case II is more likely to happen when w_i is more dissimilar to some other user's watermark, i.e., when $\underline{\alpha}_i = \min_{j \in \{1, 2, \dots, s\} / \{i\}} BA(w_i, w_j)$ is smaller. This is because the fact that $D(C)$ is dissimilar to w_i and w_i is dissimilar to some other user's watermark implies that $D(C)$ is similar to some other user's watermark. Formally, we can derive a lower bound of TDR_i as follows:

Theorem 1 (Lower bound of TDR_i). *Suppose we are given s users with any s watermarks $W = \{w_1, w_2, \dots, w_s\}$. When the watermarking method is β_i -accurate for user U_i 's AI-generated content, we have a lower bound of TDR_i :*

$$TDR_i \geq \Pr(n_i \geq \tau n) + \Pr(n_i \leq n - \tau n - \underline{\alpha}_i n), \quad (7)$$

where n_i follows a binomial distribution with parameters n and β_i , i.e., $n_i \sim B(n, \beta_i)$, $\underline{\alpha}_i = \min_{j \in \{1, 2, \dots, s\} / \{i\}} BA(w_i, w_j)$, n is the watermark length, and $0.5 < \tau < \beta_i$.

The two terms in the lower bound respectively bound the probabilities for Case I and Case II of correctly detecting user U_i 's AI-generated content. Based on Theorem 1, we have the following corollary.

Corollary 1. *When the watermarking method is more accurate, the lower bound of TDR_i is larger.*

Deriving an upper bound of FDR: Intuitively, a non-AI-generated content $C \sim \mathcal{Q}$ is also incorrectly detected as AI-generated in two cases: 1) the decoded watermark $D(C)$ is similar enough with some user's watermark, e.g., w_1 ; and 2) $D(C)$ is dissimilar to w_1 but similar enough to some other user's watermark. Based on this intuition, we can derive an upper bound of FDR as follows:

Theorem 2 (Upper bound of FDR). *Suppose we are given s users with s watermarks $W = \{w_1, w_2, \dots, w_s\}$ and watermark w_1 is selected uniformly at random. We have an upper bound of FDR as follows:*

$$FDR \leq \Pr(n_1 \geq \tau n) + \Pr(n_1 \leq n - \tau n + \overline{\alpha}_1 n), \quad (8)$$

where n_1 follows a binomial distribution with parameters n and 0.5 , i.e., $n_1 \sim B(n, 0.5)$, and $\overline{\alpha}_1 = \max_{j \in \{2, 3, \dots, s\}} BA(w_1, w_j)$.

Note that the upper bound of FDR in Theorem 2 does not depend on γ -random watermarking since we consider w_1 is picked uniformly at random. However, we found such upper bound is loose. This is because the second term of the upper bound considers the worst-case scenario of the s watermarks. The next theorem shows that when the s watermarks are constrained, in particular selected independently, we can derive a tighter upper bound of FDR.

Theorem 3 (Alternative upper bound of FDR). *Suppose we are given s users with s watermarks $W = \{w_1, w_2, \dots, w_s\}$ selected independently. When the watermarking method is γ -random for non-AI-generated content, we have an upper bound of FDR as follows:*

$$FDR \leq 1 - \Pr(n' < \tau n)^s, \quad (9)$$

where $n' \sim B(n, 0.5 + \gamma)$.

Based on Theorem 3, we have the following corollary.

Corollary 2. *When the watermarking method is more random for non-AI-generated content, i.e., γ is closer to 0, the upper bound of FDR is smaller.*

Impact of s on the bounds: Intuitively, when there are more users, i.e., s is larger, it is more likely to have at least one user whose watermark has a bitwise accuracy with the decoded watermark $D(C)$ that is no smaller than τ . As a result, both TDR_i and FDR may increase as s increases, i.e., s controls a trade-off between TDR_i and FDR. Our theoretical results align with this intuition. On one hand, our Theorem 1 shows that the lower bound of TDR_i is larger when s is larger. In particular, when s increases, the parameter α_i may become smaller. Therefore, the second term of the lower bound increases, leading to a larger lower bound of TDR_i . On the other hand, the upper bound of FDR in both Theorem 2 and Theorem 3 increases as s increases. In particular, in Theorem 2, the parameter $\overline{\alpha}_1$ becomes larger when s increases, leading to a larger second term of the upper bound.

User-agnostic vs. user-aware detection: Existing watermark-based detection is user-agnostic, i.e., it does not distinguish between different users when embedding a watermark into an AI-generated content. The first term of the lower bound in our Theorem 1 is a lower bound of TDR for user-agnostic detection; the first term of the upper bound in our Theorem 2 is an upper bound of FDR for user-agnostic detection; and the upper bound with $s = 1$ in our Theorem 3 is an alternative upper bound of FDR for user-agnostic detection. Therefore, compared to user-agnostic detection, our user-aware detection achieves larger TDR but also larger FDR.

5.5 Attribution Performance

Suppose we are given a user U_i 's AI-generated content $C \sim \mathcal{P}_i$. Intuitively, if the watermark w_i is very dissimilar to the other $s - 1$ watermarks, i.e., $\overline{\alpha}_i = \max_{j \in \{1, 2, \dots, s\} / \{i\}} BA(w_i, w_j)$ is small, then C can be correctly attributed to U_i once C is detected as AI-generated, i.e., the decoded watermark $D(C)$ is similar enough to w_i . If the watermark w_i is similar to some other watermark, i.e., $\overline{\alpha}_i$ is large, then the decoded watermark $D(C)$ has to be very similar to w_i in order to correctly attribute C to U_i . Formally, we can derive a lower bound of TAR_i in the following theorem.

Theorem 4 (Lower bound of TAR_i). *Suppose we are given s users with any s watermarks $W = \{w_1, w_2, \dots, w_s\}$. When the watermarking method is β_i -accurate for user U_i 's AI-generated content, we have a lower bound of TAR_i as follows:*

$$TAR_i \geq Pr(n_i \geq \max\{\lfloor \frac{1 + \bar{\alpha}_i}{2} n \rfloor + 1, \tau n\}), \quad (10)$$

where n_i follows a binomial distribution with parameters n and β_i , i.e., $n_i \sim B(n, \beta_i)$, $\bar{\alpha}_i = \max_{j \in \{1, 2, \dots, s\} / \{i\}} BA(w_i, w_j)$, n is the watermark length, and τ is the detection threshold.

Our Theorem 4 shows that the lower bound of TAR_i is larger when β_i is closer to 1, i.e., attribution performance is better when the watermarking method is more accurate. Moreover, the lower bound is larger when $\bar{\alpha}_i$ is smaller because it is easier to distinguish between users. This is a theoretical motivation on why our watermark selection problem aims to select watermarks for the users such that they have small pairwise bitwise accuracy.

Detection implies attribution: When $\tau > \frac{1 + \bar{\alpha}_i}{2}$, the lower bound of TAR_i in Theorem 4 becomes $TAR_i \geq Pr(n_i \geq \tau n)$. The second term of the lower bound of TDR_i in Theorem 1 is usually much smaller than the first term. In other words, the lower bound of TDR_i is also roughly $Pr(n_i \geq \tau n)$. Therefore, when τ is large enough (i.e., $> \frac{1 + \bar{\alpha}_i}{2}$), TDR_i and TAR_i are very close, which is also confirmed in our experiments. This result indicates that once an AI-generated content is correctly detected, it would also be correctly attributed.

6 Selecting Watermarks for Users

Our Theorems 1 and 4 reveal that detection and attribution performance improves when users' watermarks are more dissimilar. Leveraging this theoretical insight, we formulate the watermark selection problem, which aims to assign the most dissimilar watermarks to users. However, we demonstrate that this problem is NP-hard by reducing the well-known farthest string problem to it. This NP-hardness highlights the difficulty of developing an efficient exact solution. Consequently, we propose an efficient approximate solution to address the challenge.

6.1 Formulating a Watermark Selection Problem

Intuitively, if two users have similar watermarks, then it is hard to distinguish between them for the attribution. An extreme example is that two users have the same watermark, making it impossible to attribute either of them. In fact, our theoretical analysis in Section 5 shows that attribution performance is better if the maximum pairwise bitwise accuracy between the users' watermarks is smaller. Thus, to enhance attribution, we aim to select watermarks for the s users to minimize their maximum pairwise bitwise accuracy. Formally, we formulate watermark selection as the following optimization problem:

$$\min_{w_1, w_2, \dots, w_s} \max_{i, j \in \{1, 2, \dots, s\}, i \neq j} BA(w_i, w_j), \quad (11)$$

where BA stands for bitwise accuracy between two watermarks. This optimization problem jointly optimizes the s watermarks simultaneously. As a result, it is very challenging to solve the optimization problem because the GenAI service provider does not know the number of registered users (i.e., s) in advance. In practice, users register in the GenAI service at very different times. To address the challenge, we select a watermark for a user at the time of his/her registration in the GenAI service. For the first user U_1 , we select a watermark uniformly at random. Suppose we have selected watermarks for $s - 1$ users. Then, the s th user registers and we aim to select a watermark w_s whose maximum bitwise accuracy with the existing $s - 1$ watermarks is minimized. Formally, we formulate a *watermark selection problem* as follows:

$$\min_{w_s} \max_{i \in \{1, 2, \dots, s-1\}} BA(w_i, w_s). \quad (12)$$

6.2 Solving the Watermark Selection Problem

NP-hardness: We can show that our watermark selection problem in Equation 12 is NP-hard. In particular, we can reduce the well-known *farthest string problem* [18], which is NP-hard, to our watermark selection problem. In the farthest string problem, we aim to find a string that is the farthest from a given set of strings. We can view a string as a watermark in our watermark selection problem, the given set of strings as the watermarks of the $s - 1$ users, and the similarity metric between two strings as our bitwise accuracy. Then, we can reduce the farthest string problem to our watermark selection problem, which means that our watermark selection problem is also NP-hard. This NP-hardness

Table 1: The maximum pairwise bitwise accuracy among the watermarks generated by NRG and A-BSTA for different initializations.

	$\neg w_1$ initialization	Random initialization
NRG	0.766	0.750
A-BSTA	0.875	0.734

implies that it is very challenging to develop an efficient exact solution for our watermark selection problem. We note that efficiency is important for watermark selection as we aim to select a watermark for a user at the time of registration. Thus, we aim to develop an *efficient* algorithm that *approximately* solves the watermark selection problem.

Random: The most straightforward method to approximately solve the watermark selection problem in Equation 12 is to generate a watermark uniformly at random as w_s . We denote this method as *Random*. The limitation of this method is that the selected watermark w_s may be very similar to some existing watermarks, i.e., $\max_{i \in \{1, 2, \dots, s-1\}} BA(w_i, w_s)$ is large, making attribution less accurate, as shown in our experiments.

Decision problem: To develop an efficient algorithm to approximately solve our watermark selection problem, we first define its *decision problem*. Specifically, given the maximum number of matched bits between w_s and the existing $s - 1$ watermarks as m , the decision problem aims to find such a w_s if there exists one and return *NotExist* otherwise. Formally, the decision problem is to find any watermark w_s in the following set if the set is nonempty: $w_s \in \{w \mid \max_{i \in \{1, 2, \dots, s-1\}} BA(w_i, w) \leq m/n\}$, where n is the watermark length. Next, we discuss how to solve the decision problem and then turn the algorithm to solve our watermark selection problem.

Bounded search tree algorithm (BSTA) [19]: Recall that our watermark selection problem is equivalent to the farthest string problem. Thus, our decision problem is equivalent to that of the farthest string problem, which has been studied extensively in the theoretical computer science community. In particular, BSTA is the state-of-the-art *exact* algorithm to solve the decision problem version of the farthest string problem. We apply BSTA to solve the decision problem version of our watermark selection problem exactly, which is shown in Algorithm 1 in Appendix. The key idea of BSTA is to initialize w_s as $\neg w_1$ (i.e., each bit of w_1 flips), and then reduce the decision problem to a simpler problem recursively until it is easily solvable or there does not exist a solution w_s . In particular, given an initial w_s , BSTA first finds the existing watermark w_{i^*} that has the largest bitwise accuracy with w_s . If $BA(w_{i^*}, w_s) \leq m/n$, then w_s is already a solution to the decision problem and thus BSTA returns w_s . Otherwise, BSTA chooses any $m + 1$ bits that w_s and w_{i^*} match. For each of the chosen $m + 1$ bits, BSTA flips the corresponding bit in w_s and recursively solves the decision problem using the new w_s as an initialization. The recursion is applied m times at most, i.e., the recursion depth d is set as m when calling Algorithm 1 in Appendix.

A key limitation of BSTA is that it has an exponential time complexity [19]. In fact, since the decision problem is NP-hard, all known *exact* solutions have exponential time complexity. Therefore, to enhance computation efficiency, we resort to approximate solutions. Next, we discuss the state-of-the-art approximate solution that adapts BSTA and a new approximate solution that we propose.

Non Redundant Guess (NRG) [32]: Like BSTA, this approximate solution also first initializes w_s as $\neg w_1$ and finds the existing watermark w_{i^*} that has the largest bitwise accuracy with w_s . If $BA(w_{i^*}, w_s) \leq m/n$, then NRG returns w_s . Otherwise, NRG samples $n \cdot BA(w_{i^*}, w_s) - m$ bits that w_s and w_{i^*} match uniformly at random. Then, NRG flips these bits in w_s and recursively solve the decision problem using the new w_s as an initialization. Note that NRG stops the recursion when m bits of the initial w_s have been flipped. Algorithm 2 in Appendix shows NRG.

Approximate bounded search tree algorithm (A-BSTA): We adapt BSTA as an efficient approximate solution to our decision problem. Specifically, A-BSTA makes two adaptations of BSTA. First, we constrain the recursion depth d to be a constant (e.g., 8 in our experiments) instead of m , which makes the algorithm approximate but improves the efficiency substantially. Second, instead of initializing w_s as $\neg w_1$, we initialize w_s as a uniformly random watermark. As our experiments in Table 1 show, our initialization further improves the performance of A-BSTA. This is because a random initialization is more likely to have small bitwise accuracy with all existing watermarks. Note that BSTA, NRG, and A-BSTA all return *NotExist* if they cannot find a solution w_s to the decision problem.

Solving our watermark selection problem: Given an algorithm (e.g., BSTA, NRG, or A-BSTA) to solve the decision problem, we turn it as a solution to our watermark selection problem. Specifically, our idea is to start from a small m , and then solve the decision problem. If we cannot find a watermark w_s for the given m , we increase it by 1 and solve the decision problem again. We repeat this process until finding a watermark w_s . Note that we start from $m = \max_{i \in \{1, 2, \dots, s-2\}} n \cdot BA(w_i, w_{s-1})$, i.e., the maximum number of matched bits between w_{s-1} and the other

$s - 2$ watermarks. This is because an m smaller than this value is unlikely to produce a watermark w_s as it failed to do so when selecting w_{s-1} . Algorithm 3 in Appendix shows our method.

Note that binary search is another way to find a proper m . Specifically, we start with a small m (denoted as m_l) that does not produce a w_s and a large m (denoted as m_u) that does produce a w_s . If $m = (m_l + m_u)/2$ produces a w_s , we update $m_u = (m_l + m_u)/2$; otherwise we update $m_l = (m_l + m_u)/2$. The search process stops when $m_l \geq m_u$. However, we found that increasing m by 1 as in our Algorithm 3 in Appendix is more efficient than binary search. This is because increasing m by 1 expands the search space of w_s substantially, which often leads to a valid w_s . On the contrary, binary search would require solving the decision problem multiple times with different m until finding that $m + 1$ is enough.

Time complexity: We analyze the time complexity of the algorithms to solve the decision problem. For Random, the time complexity is $O(n)$. For BSTA, the time complexity to solve the decision problem with parameter m is $O(snm^m)$ according to [19]. For NRG, the time complexity is $O(sn + s\sqrt{m} \cdot 5^m)$ according to [32]. For A-BSTA, the time complexity is $O(snm^d)$, where d is a constant.

7 Experiments

In our major experiments, we focus on detection and attribution of AI-generated images. In Section 8, we also show results for AI-generated texts.

7.1 Experimental Setup

Datasets: We consider both AI-generated and non-AI-generated images as follows:

AI-generated. We consider three GenAI models, i.e., Stable Diffusion, Midjourney, and DALL-E 2, which correspond to three datasets of AI-generated images. For Stable Diffusion, we use publicly available dataset DiffusionDB [33]. For Midjourney, we collect its generated images from a website [34]. For DALL-E 2, we also collect its generated images from a website [35]. Following HiDDeN [7], for each dataset, we sample 10,000 images for training watermark encoders and decoders; and we sample 1,000 images for testing the performance of watermark-based detection and attribution.

Non-AI-generated. To evaluate the likelihood that a non-AI-generated image is falsely detected as AI-generated, we need non-AI-generated images. For this purpose, we combine the images in three benchmark datasets, including COCO [36], ImageNet [37], and Conceptual Caption [38], and sample 1,000 images from the combined set uniformly at random as our non-AI-generated image dataset.

We scale the image size in all datasets to be 128×128 .

Watermarking method: We use the learning-based watermarking method HiDDeN [7], which is the basis for modern learning-based image watermarking. Unless otherwise mentioned, we use standard training with the default parameter settings in the publicly available code, except that we use ResNet18 as the decoder to enlarge the capacity to encode/decode longer watermarks. For each GenAI model, we train a watermark encoder/decoder using the corresponding AI-generated image training set and evaluate the detection and attribution performance on the testing set.

Watermark selection methods: We evaluate Random, NRG, and A-BSTA watermark selection methods. Unless otherwise mentioned, we use A-BSTA. Note that we do not use BSTA because it is not scalable. For instance, it takes BSTA more than 8 hours to generate even 16 watermarks.

Evaluation metrics: As discussed in Section 5.2, we mainly use three evaluation metrics, i.e., TDR, FDR, and TAR. FDR is the fraction of the 1,000 non-AI-generated images that are falsely detected as AI-generated. FDR does not depend on users. In contrast, TDR and TAR depend on users because they use different watermarks, leading to different distributions of AI-generated images. For each of the s users, we embed its watermark into 100 images randomly sampled from a testing AI-generated image dataset; and then we calculate the TDR and TAR for the user.

In most of our experiments, we report the *average TDR* and *average TAR*, which respectively are the TDR and TAR averaged among the s users. However, average TDR and average TAR cannot reflect the detection/attribution performance for the worst-case users, i.e., some users may have quite small TDR/TAR, but the average TDR/TAR may still be very large. Therefore, we further consider the 1% users (at least 1 user) with the smallest TDR (or TAR) and report their average TDR (or TAR), which we call *worst 1% TDR* (or *worst 1% TAR*).

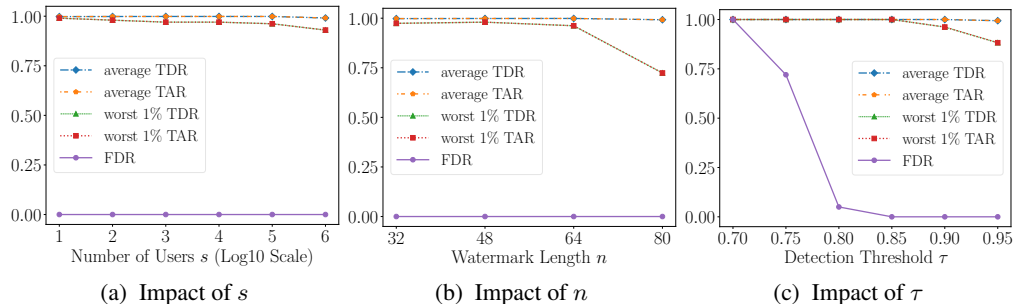


Figure 3: Impact of number of users s , watermark length n , and detection threshold τ on detection and attribution performance.

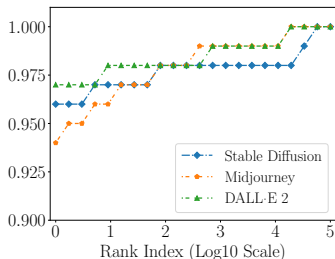


Figure 4: Ranked TARs of the 100,000 users.

Table 2: The average β_i of all users and of the worst 1% of users, where β_i of a user is estimated using the testing images.

Watermark Length n	32	48	64	80
Average β_i	0.99	0.99	0.99	0.97
Worst 1% β_i	0.92	0.97	0.90	0.84

Parameter settings: By default, we set the number of users $s = 100,000$, watermark length $n = 64$, and detection threshold $\tau = 0.9$. To compute TAR of an user, we need to compute the bitwise accuracy between the decoded watermark and each user’s watermark for each watermarked image, and thus we set $s = 100,000$ due to our limited computation resources, but we will also explore $s = 1,000,000$ in one of our experiments to show the results when the number of users in attribution is very large. When post-processing methods are applied to watermarked images, the watermarking method may become less accurate (i.e., β may decrease) and thus we reduce τ to be 0.85. Unless otherwise mentioned, we show results for the Stable Diffusion dataset.

7.2 Without Post-processing

In this section, we show results when the AI-generated, watermarked images are not post-processed. Specifically, we explore the impact of the three parameters, including the number of users s , watermark length n , and detection threshold τ , on the detection and attribution performance. When exploring the impact of one parameter, we fix the other two parameters as their default settings.

Main results: For each GenAI model, we compute the TDR/TAR of each user and the FDR. The FDRs for the three GenAI models are nearly 0. Then, we rank the users’ TARs (or TDRs) in a non-descending order. Figure 4 shows the ranked TARs of the 100,000 users for the three GenAI models. Note that the curve of TDR overlaps with that of TAR for a GenAI model and thus is omitted in the figure for simplicity. TDR and TAR overlap because $\tau = 0.9 > \frac{1+\alpha_i}{2}$ (0.89 in our experiments), which is consistent with our theoretical analysis in Section 5.5 that shows detection implies attribution in such settings. Our results show that watermark-based detection and attribution are accurate when the AI-generated, watermarked images are not post-processed. Specifically, the worst TAR or TDR of a user is larger than 0.94; less than 0.1% of users have TARs/TDRs smaller than 0.98; and 85% of users have TARs/TDRs of 1 for Midjourney and DALL-E 2, and 60% of users have TARs/TDRs of 1 for Stable Diffusion.

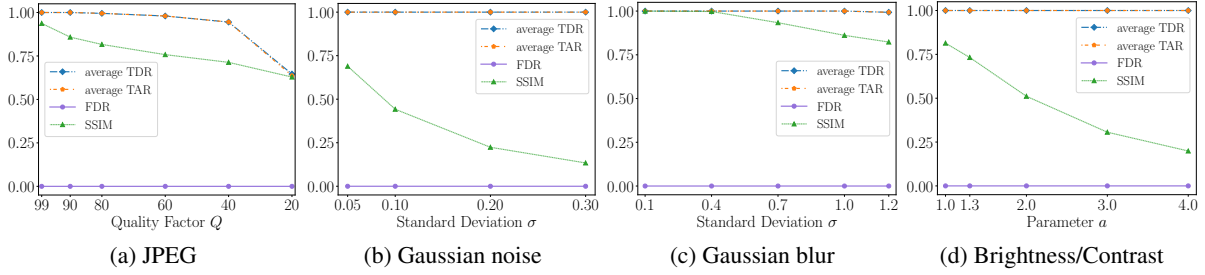


Figure 5: Detection and attribution results when AI-generated and non-AI-generated images are post-processed by common post-processing methods with different parameters. SSIM measures the quality of an image after post-processing.

Impact of number of users s : Figure 3a shows the average TDR, average TAR, worst 1% TDR, worst 1% TAR, and FDR when s varies from 10 to 1,000,000. We have two observations. First, both average TDR and average TAR are consistently close to 1, and FDR is consistently close to 0, which means our detection and attribution are accurate. Second, worst 1% TDR and worst 1% TAR decrease as s increases. This is because when there are more users, the worst 1% of them have smaller TDRs and TARs. Moreover, these worst 1% of users also make the average TDR and average TAR decrease slightly when s increases from 100,000 to 1,000,000.

Impact of watermark length n : Figure 3b shows the average TDR, average TAR, worst 1% TDR, worst 1% TAR, and FDR when the watermark length n varies from 32 to 80. The average TDR and average TAR slightly decrease when n increases from 64 to 80, while the worst 1% TDR/TAR slightly increases as n increases from 32 to 48 and then decreases as n further increases. Table 2 shows the estimated average β_i of all users and average β_i of the worst 1% of users in β -accurate watermarking. We observe that the patterns of average TDR/TAR and worst 1% TDR/TAR are consistent with those of average β_i and worst 1% β_i , respectively. These observations are consistent with our theoretical analysis which shows that TDR or TAR increases as β_i increases. Our result also implies that HiDDeN watermarking may be unable to accurately encode/decode very long watermarks.

Impact of detection threshold τ : Figure 3c shows the average TDR, average TAR, worst 1% TDR, worst 1% TAR, and FDR when the detection threshold τ varies from 0.7 to 0.95. When τ increases, both TDR and TAR decrease, while FDR also decreases. Such trade-off of τ is consistent with Theorem 1, 3, and 4.

7.3 Common Post-processing

Common post-processing methods: Common post-processing methods are often used to evaluate the robustness of watermarking in *non-adversarial settings*. Each post-processing method has specific parameters that govern the extent of perturbation introduced to an image. In particular, we consider common post-processing methods as follows.

JPEG. JPEG [39] method compresses an image via a discrete cosine transform. The perturbation introduced to an image is determined by the *quality factor* Q . An image is perturbed more when Q is smaller.

Gaussian noise. This method perturbs an image via adding a random Gaussian noise to each pixel. In our experiments, the mean of the Gaussian distribution is 0. The perturbation introduced to an image is determined by the parameter *standard deviation* σ .

Gaussian blur. This method blurs an image via a Gaussian function. In our experiments, we fix kernel size $s = 5$. The perturbation introduced to an image is determined by the parameter *standard deviation* σ .

Brightness/Contrast. This method perturbs an image via adjusting the brightness and contrast. Formally, the method has contrast parameter a and brightness parameter b , where each pixel x is converted to $ax + b$. In our experiments, we fix $b = 0.2$ and vary a to control the perturbation.

Adversarial training [7]: We use adversarial training to train HiDDeN. Specifically, during training, we randomly sample a post-processing method from no post-processing and common post-processing with a random parameter to post-process each watermarked image in a mini-batch. Following previous work [7], we consider the following range of parameters during adversarial training: $Q \in [10, 99]$ for JPEG, $\sigma \in [0, 0.5]$ for Gaussian noise, $\sigma \in [0, 1.5]$ for Gaussian blur, and $a \in [1, 20]$ for Brightness/Contrast.

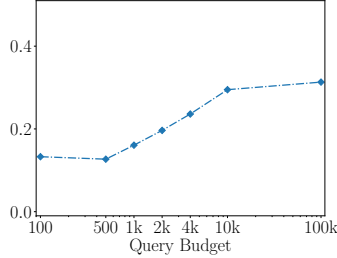


Figure 6: Average SSIM between watermarked images and their adversarially post-processed versions as a function of the query budget in the black-box setting.

Table 3: The average running time for different watermark selection methods to generate a watermark.

	Random	NRG	A-BSTA
Time (ms)	0.01	2.11	24.00

Results: Figure 5 shows the detection/attribution results when a common post-processing method with different parameters is applied to the (AI-generated and non-AI-generated) images. SSIM [40] is a popular metric to measure visual similarity between two images. The SSIM in Figure 5 is the average between (AI-generated and non-AI-generated) images and their post-processed versions. We note that when HiDDeN is trained using standard training, detection and attribution become inaccurate after AI-generated images are post-processed, as shown in Figure 10 in Appendix. Our results show that detection and attribution using an adversarially trained HiDDeN are robust to common post-processing. In particular, the average TDR and TAR are still high when a common post-processing does not sacrifice image quality substantially. For instance, average TDR and TAR start to decrease when the quality factor Q of JPEG is smaller than 90. However, the average SSIM between watermarked images and their post-processed versions also drops quickly. Note that Gaussian blur with $\sigma = 1.2$ already influences visual quality substantially even if SSIM is larger than 0.75. Figure 11 in Appendix shows a watermarked image and the versions post-processed by different methods.

7.4 Adversarial Post-processing

In adversarial settings, an attacker may apply adversarial post-processing to perturb watermarked images to evade detection/attribution. HiDDeN is not robust to adversarial post-processing in the white-box setting [13], i.e., watermark can be removed from a watermarked image without sacrificing its visual quality. Thus, HiDDeN-based detection/attribution is also not robust to adversarial post-processing in the white-box setting, i.e., TDR/TAR can be reduced to 0 while maintaining image quality.

Figure 6 shows the average SSIM between watermarked images and their adversarially post-processed versions as a function of query budget in the black-box setting (i.e., WEvade-B-Q [13]), where the query budget is the number of queries to the detection API for *each* watermarked image. HiDDeN is trained via adversarial training in these experiments. Both TDR and TAR are 0 in these experiments since WEvade-B-Q always guarantees evasion [13]. However, adversarial post-processing substantially sacrifices image quality in the black-box setting (i.e., SSIM is small) even if an attacker can query the detection API for a large number of times. Figure 12 in Appendix shows several examples of adversarially post-processed images with degraded visual quality. Our results show that HiDDeN and thus our HiDDeN-based detection/attribution have good robustness to adversarial post-processing in the black-box setting.

We note that Jiang et al. [13] showed adversarial post-processing does not sacrifice image visual quality in the black-box setting when evading HiDDeN, which we can reproduce using their publicly available code and the same parameter setting. However, they use watermark length 30, while we use 64; and they use a simple neural network as the decoder, while we use ResNet18 as the decoder. Moreover, we use stronger adversarial training with a larger range of parameters for the post-processing. Our results show that longer watermarks, more expressive decoder, and stronger adversarial training can further enhance robustness of HiDDeN.

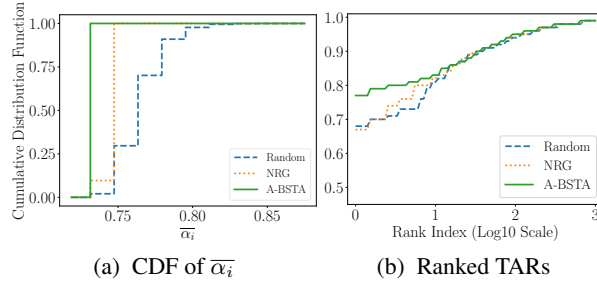


Figure 7: (a) The cumulative distribution function (CDF) of $\bar{\alpha}_i$ and (b) ranked TARs of the worst 1,000 users for the three watermark selection methods.

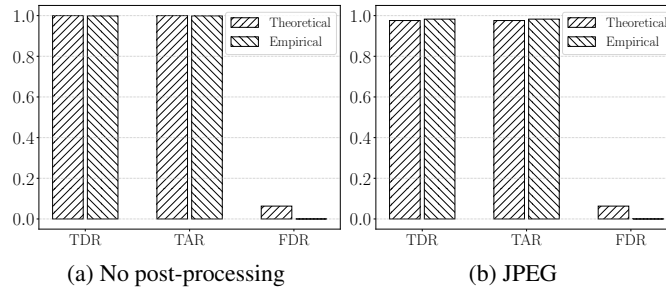


Figure 8: Theoretical vs. empirical results.

Table 4: Theoretical lower bounds of TDR/TAR and upper bound of FDR when there are 100 million users.

bound of TDR	bound of FDR	bound of TAR
99.99%	6.00%	99.99%

7.5 Different Watermark Selection Methods

Running time: Table 3 shows the running time to generate a watermark averaged among the 100,000 watermarks. Although A-BSTA is slower than Random and NRG, the running time is acceptable, i.e., it takes only 24ms to generate a watermark on average.

Distribution of $\bar{\alpha}_i$: Recall that TAR_i of a user depends on the maximum bitwise accuracy between the watermark w_i and the remaining watermarks, i.e., $\bar{\alpha}_i = \max_{j \in \{1, 2, \dots, s\} / \{i\}} \text{BA}(w_i, w_j)$. Figure 7a shows the *cumulative distribution function* of $\bar{\alpha}_i$ among the s watermarks generated by different watermark selection methods. Our results show that all watermarks generated by A-BSTA have $\bar{\alpha}_i$ smaller than 0.74. However, Random and NRG generate many watermarks with larger $\bar{\alpha}_i$, and Random is the worst among the three methods. This is because Random does not explicitly minimize $\bar{\alpha}_i$ when generating watermarks.

TARs: Figure 7b shows the ranked TARs of the worst 1,000 users, where the AI-generated images are post-processed by JPEG compression with quality factor $Q = 90$ and HiDDeN is adversarially trained. The results indicate that A-BSTA outperforms NRG, which outperforms Random. This is because A-BSTA selects watermarks with smaller $\bar{\alpha}_i$, while Random selects watermarks with larger $\bar{\alpha}_i$ as shown in Figure 7a.

7.6 Theoretical vs. Empirical Results

The theoretical lower bounds of TDR and TAR of a user are respectively calculated using Theorem 1 and 4, while the theoretical upper bound of FDR is calculated using Theorem 3. We estimate β_i as the bitwise accuracy between the decoded watermark and w_i averaged among the testing AI-generated images, and estimate γ using the fraction of bits in the decoded watermarks that are 1 among the non-AI-generated images. Figure 8 shows the average theoretical vs. empirical TDR/TAR, and theoretical vs. empirical FDR, when no post-processing or JPEG with $Q = 90$ is applied. The results show that our theoretical lower bounds of TDR and TAR match with empirical results well, which indicates

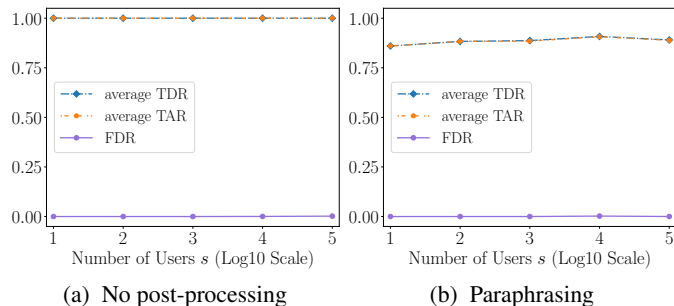


Figure 9: Results of watermark-based detection and attribution for AI-generated texts.

that our derived lower bounds are tight. The theoretical upper bound of FDR is notably higher than the empirical FDR. This is because some bits may have larger probabilities to be 1 or 0 in the experiments, but our theoretical analysis treats bits equally, leading to a loose upper bound of FDR.

Theoretical results when there are 100 million users: Due to limited computational resources, we cannot empirically evaluate detection and attribution performance for 100 million users. Instead, we show theoretical results on 100 million users in Table 4, assuming $\beta_i = 0.99$, $\underline{\alpha}_i = 0.2$, $\gamma = 0.05$, and $\bar{\alpha}_i = 0.8$. We notice that TDR and TAR remain very close to 1.

8 Discussion and Limitations

AI-generated texts: Our method can also be used for the detection and attribution of AI-generated texts. For text watermarking, we use a learning-based method called *Adversarial Watermarking Transformer (AWT)* [22]. Given a text, AWT encoder embeds a watermark into it; and given a (watermarked or unwatermarked) text, AWT decoder decodes a watermark from it. Following the original paper [22], we train AWT on the word-level WikiText-2 dataset, which is derived from Wikipedia articles [41]. We use most of the hyperparameter settings in the publicly available code of AWT except the weight of the watermark decoding loss. To optimize watermark decoding accuracy, we increase this weight during training. The detailed hyperparameter settings for training can be found in Table 5 in Appendix.

We use A-BSTA to select users’ watermarks. For each user, we sample 10 text segments from the test corpus uniformly at random, and perform watermark-based detection and attribution. Moreover, we use the unwatermarked test corpus to calculate FDR. Figure 9 shows the detection and attribution results when there is no post-processing and *paraphrasing* [42] is applied to texts, where $n = 64$, $\tau = 0.85$, and s ranges from 10 to 100,000. Due to the fixed-length nature of AWT’s input, we constrain the output length of the paraphraser to a certain range. When paraphrasing is used, we extend adversarial training to train AWT, and Section .7 in Appendix shows the details. Note that the average TDR/TAR and FDR are all nearly 0 when AWT is trained by standard training and paraphrasing is applied to texts. The results show that our method is also applicable for AI-generated texts, and adversarially trained AWT has better robustness to paraphrasing.

Attribution of GenAI services: In this work, we focus on attribution of content to users for a specific GenAI service. Another relevant attribution problem is to trace back the GenAI service (e.g., Google’s Imagen, OpenAI’s DALL-E 3, or Stable Diffusion) that generated a given content. Our method can also be applied to such GenAI-service-attribution problem by assigning a different watermark to each GenAI service. When GenAI service generates content, its corresponding watermark is embedded into it. Then, our method can be applied to detect whether a content is AI-generated and further attribute the GenAI service if the content is detected as AI-generated.

In service attribution, selecting watermarks for different GenAI services can be coordinated by a central authority, who runs our watermark selection algorithm to pick unique watermarks for the GenAI services. A GenAI service registers to the central authority in order to obtain a unique watermark. Such a central authority is similar to the certificate authority in the Public Key Infrastructure (PKI) that is widely used to secure communications on the Internet. The central authority may also perform detection and attribution of AI-generated content since it has access to all GenAI services’ watermarks. However, the central authority may become a bottleneck in such detection and attribution. To mitigate this issue, the watermarks of all GenAI services can be shared with each GenAI service, so each GenAI service

can perform detection and attribution. We note that a central authority is not needed in user attribution of a particular GenAI service. This is because the GenAI service can select watermarks for its users and perform detection/attribution.

Hierarchical attribution: We can perform attribution to GenAI service and user simultaneously. Specifically, we can divide the watermark space into multiple subspaces; and each GenAI service uses a subspace of watermarks and assigns watermarks in its subspace to its users. In this way, we can trace back both the GenAI service and its user that generated a given content.

9 Conclusion and Future Work

We show that watermarks can be effectively used for user-aware detection and attribution of AI-generated content. The main challenge in this approach is how to select watermarks for users to maximize detection and attribution performance. We show that this challenge can be addressed through a two-step solution. First, we theoretically derive the detection and attribution performance for any given set of user watermarks. Second, we select user watermarks to maximize the theoretical performance. Our empirical evaluation shows that, using the current state-of-the-art watermarking method, detection and attribution are highly accurate when the watermarked AI-generated content is either not post-processed, subjected to common post-processing, or exposed to black-box adversarial post-processing with limited query budgets. An important direction for future work is to develop robust watermarking methods in adversarial settings, which would enhance the robustness of watermark-based detection and attribution in such contexts.

References

1. Dhaliwal, S. *Elon Musk isn't dating GM's Mary Barra: he has this to say though on the photos*. <https://www.benzinga.com/news/23/03/31505898/elon-musk-isnt-dating-gms-mary-barra-he-has-this-to-say-though-on-the-photos>. 2023.
2. Escalante-De Mattei, S. *US Copyright Office: AI Generated Works Are Not Eligible for Copyright*. <https://www.artnews.com/art-news/news/ai-generator-art-text-us-copyright-policy-1234661683>. 2023.
3. Pereira, S. & Pun, T. Robust Template Matching for Affine Resistant Image Watermarks. *IEEE Transactions on Image Processing* (2000).
4. Bi, N., Sun, Q., Huang, D., Yang, Z. & Huang, J. Robust Image Watermarking based on Multiband Wavelets and Empirical Mode Decomposition. *IEEE Transactions on Image Processing* (2007).
5. Wang, Q. *Invisible Watermark*. <https://github.com/ShieldMnt/invisible-watermark>. 2021.
6. Kandi, H., Mishra, D. & Gorthi, S. R. S. Exploring the Learning Capabilities of Convolutional Neural Networks for Robust Image Watermarking. *Computers & Security* (2017).
7. Zhu, J., Kaplan, R., Johnson, J. & Fei-Fei, L. *Hidden: Hiding Data with Deep Networks* in *European Conference on Computer Vision* (2018).
8. Luo, X., Zhan, R., Chang, H., Yang, F. & Milanfar, P. *Distortion Agnostic Deep Watermarking* in *IEEE/CVF Conference on Computer Vision and Pattern Recognition* (2020).
9. Wen, B. & Aydore, S. *Romark: A Robust Watermarking System using Adversarial Training* in *Conference on Neural Information Processing Systems Workshop* (2019).
10. Fernandez, P., Couairon, G., Jégou, H., Douze, M. & Furon, T. *The Stable Signature: Rooting Watermarks in Latent Diffusion Models* in *International Conference on Computer Vision* (2023).
11. Lukas, N. & Kerschbaum, F. PTW: Pivotal Tuning Watermarking for Pre-Trained Image Generators. *USENIX Security Symposium* (2023).
12. Jiang, Z., Guo, M., Hu, Y., Jia, J. & Gong, N. Z. *Certiably Robust Image Watermark* in *European Conference on Computer Vision* (2024).
13. Jiang, Z., Zhang, J. & Gong, N. Z. *Evading Watermark based Detection of AI-Generated Content* in *ACM Conference on Computer and Communications Security* (2023).
14. Ramesh, A., Dhariwal, P., Nichol, A., Chu, C. & Chen, M. Hierarchical Text-Conditional Image Generation with Clip Latents. *arXiv preprint arXiv:2204.06125* (2022).
15. Gowal, S. & Kohli, P. *Identifying AI-generated Images with SynthID*. <https://deepmind.google/discover/blog/identifying-ai-generated-images-with-synthid>. 2023.
16. Rombach, R., Blattmann, A., Lorenz, D., Esser, P. & Ommer, B. *High-Resolution Image Synthesis with Latent Diffusion Models* in *IEEE/CVF Conference on Computer Vision and Pattern Recognition* (2022).

17. Mehdi, Y. *Announcing Microsoft Copilot, Your Everyday AI Companion*. <https://blogs.microsoft.com/blog/2023/09/21/announcing-microsoft-copilot-your-everyday-ai-companion>. 2023.
18. Lanctot, J. K., Li, M., Ma, B., Wang, S. & Zhang, L. Distinguishing String Selection Problems. *Information and Computation* (2003).
19. Gramm, J., Niedermeier, R. & Rossmann, P. Fixed-Parameter Algorithms for Closest String and Related Problems. *Algorithmica* (2003).
20. Wen, Y., Kirchenbauer, J., Geiping, J. & Goldstein, T. *Tree-Ring Watermarks: Fingerprints for Diffusion Images that are Invisible and Robust* in *Conference on Neural Information Processing Systems* (2023).
21. Kirchenbauer, J. *et al.* A Watermark for Large Language Models in *International Conference on Machine Learning* (2023).
22. Abdelnabi, S. & Fritz, M. *Adversarial Watermarking Transformer: Towards Tracing Text Provenance with Data Hiding* in *IEEE Symposium on Security and Privacy* (2021).
23. Tancik, M., Mildenhall, B. & Ng, R. *Stegastamp: Invisible hyperlinks in physical photographs* in *IEEE/CVF Conference on Computer Vision and Pattern Recognition* (2020).
24. Goodfellow, I., Shlens, J. & Szegedy, C. *Explaining and Harnessing Adversarial Examples* in *International Conference on Learning Representations* (2015).
25. Madry, A., Makelov, A., Schmidt, L., Tsipras, D. & Vladu, A. *Towards Deep Learning Models Resistant to Adversarial Attacks* in *International Conference on Learning Representations* (2018).
26. Sadasivan, V. S., Kumar, A., Balasubramanian, S., Wang, W. & Feizi, S. Can AI-Generated Text be Reliably Detected? *arXiv preprint arXiv:2303.11156* (2023).
27. Lukas, N., Diaa, A., Fenaux, L. & Kerschbaum, F. Leveraging Optimization for Adaptive Attacks on Image Watermarks. *International Conference on Learning Representations* (2024).
28. Hu, Y., Jiang, Z., Guo, M. & Gong, N. A Transfer Attack to Image Watermarks. *arXiv preprint arXiv:2403.15365* (2024).
29. Stringhini, G. *et al.* {EVILCOHORT}: Detecting communities of malicious accounts on online services in *USENIX Security Symposium* (2015).
30. Yuan, D. *et al.* Detecting Fake Accounts in Online Social Networks at the Time of Registrations in *ACM Conference on Computer and Communications Security* (2019).
31. Xu, T. *et al.* Deep Entity Classification: Abusive Account Detection for Online Social Networks in *USENIX Security Symposium* (2021).
32. Chen, Z.-Z., Ma, B. & Wang, L. Randomized Fixed-Parameter Algorithms for the Closest String Problem. *Algorithmica* (2016).
33. Wang, Z. J. *et al.* DiffusionDB: A Large-Scale Prompt Gallery Dataset for Text-to-Image Generative Models in *Annual Meeting of the Association for Computational Linguistics* (2023).
34. Turc, I. & Nemade, G. *Midjourney User Prompts & Generated Images (250k)*. <https://www.kaggle.com/ds/2349267>. 2022.
35. Images, D. *DALLE2 Image Database*. <https://dalle2.gallery>. 2023.
36. Lin, T.-Y. *et al.* Microsoft COCO: Common Objects in Context in *European Conference on Computer Vision* (2014).
37. Deng, J. *et al.* Imagenet: A Large-Scale Hierarchical Image Database in *IEEE/CVF Conference on Computer Vision and Pattern Recognition* (2009).
38. Sharma, P., Ding, N., Goodman, S. & Soricut, R. *Conceptual Captions: A Cleaned, Hypernymed, Image Alt-text Dataset for Automatic Image Captioning* in *Annual Meeting of the Association for Computational Linguistics* (2018).
39. Zhang, C., Karjauv, A., Benz, P. & Kweon, I. S. Towards Robust Data Hiding Against (JPEG) Compression: A Pseudo-Differentiable Deep Learning Approach. *arXiv preprint arXiv:2101.00973* (2020).
40. Wang, Z., Bovik, A. C., Sheikh, H. R. & Simoncelli, E. P. Image Quality Assessment: From Error Visibility to Structural Similarity. *IEEE Transactions on Image Processing* (2004).
41. Merity, S., Xiong, C., Bradbury, J. & Socher, R. *Pointer Sentinel Mixture Models* in *International Conference on Learning Representations* (2017).
42. Damodaran, P. *Parrot: Paraphrase Generation for NLU*. version v1.0. 2021.

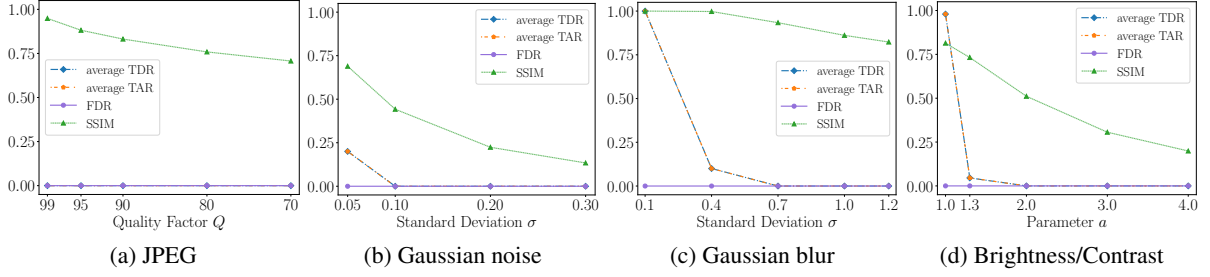


Figure 10: Detection and attribution results when AI-generated and non-AI-generated images are post-processed by common post-processing methods with different parameters. HiDDeN is trained using standard training.

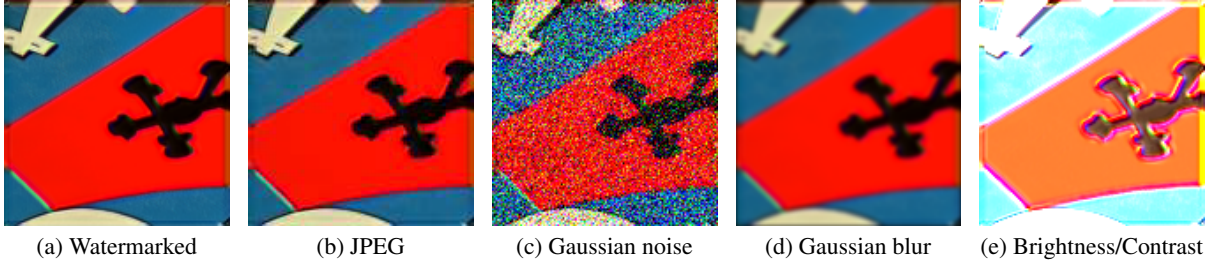


Figure 11: A watermarked image and the versions post-processed by JPEG with $Q=60$, Gaussian noise with $\sigma=0.3$, Gaussian blur with $\sigma=1.2$, and Brightness/Contrast with $a=4.0$.

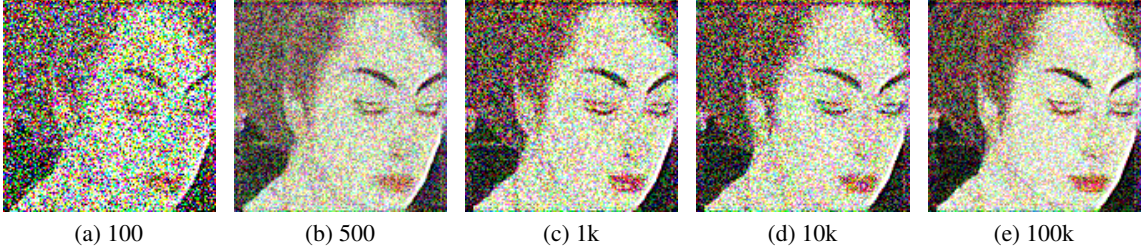


Figure 12: Perturbed watermarked images obtained by adversarial post-processing with different number of queries to the detection API in the black-box setting.

.1 Proof of Theorem 1

For $C \sim \mathcal{P}_i$, we denote $w = D(C)$, $n_i = BA(w, w_i)n$, and $n_j = BA(w, w_j)n$ for $j \in \{1, 2, \dots, s\}/\{i\}$. Then we have the following:

$$\begin{aligned} |w - \neg w_i|_1 &= n_i, \\ |\neg w_i - w_j|_1 &= BA(w_i, w_j)n, \\ |w - w_j|_1 &= n - n_j, \end{aligned}$$

where $\neg w_i$ means flipping each bit of the watermark w_i , $|\cdot|_1$ is ℓ_1 distance between two binary vectors. According to the triangle inequality, we have:

$$\begin{aligned} |w - w_j|_1 &\leq |w - \neg w_i|_1 + |\neg w_i - w_j|_1 \\ &= n_i + BA(w_i, w_j)n. \end{aligned}$$

Therefore, we derive the lower bound of n_j for $j \in \{1, 2, \dots, s\}/\{i\}$ as follows:

$$\begin{aligned} n_j &= n - |w - w_j|_1 \\ &\geq n - n_i - BA(w_i, w_j)n. \end{aligned}$$

Thus, we derive the lower bound of TDR_i as follows:

$$\begin{aligned}
TDR_i &= 1 - \Pr(n_i < \tau n \wedge \max_{j \in \{1, 2, \dots, s\} / \{i\}} n_j < \tau n) \\
&\geq 1 - \Pr(n_i < \tau n \wedge \max_{j \in \{1, 2, \dots, s\} / \{i\}} n - n_i - BA(w_i, w_j)n < \tau n) \\
&= 1 - \Pr(n_i < \tau n \wedge n - n_i - \underline{\alpha}_i n < \tau n) \\
&= 1 - \Pr(n - \tau n - \underline{\alpha}_i n < n_i < \tau n) \\
&= \Pr(n_i \geq \tau n) + \Pr(n_i \leq n - \tau n - \underline{\alpha}_i n),
\end{aligned}$$

where $n_i \sim B(n, \beta_i)$ and $\underline{\alpha}_i = \min_{j \in \{1, 2, \dots, s\} / \{i\}} BA(w_i, w_j)$.

2 Proof of Corollary 1

According to Theorem 1, the lower bound of TDR_i is $1 - \Pr(n - \tau n - \underline{\alpha}_i n < n_i < \tau n)$. For an integer $r \in (n - \tau n - \underline{\alpha}_i n, \tau n)$ and $n_i \sim B(n, \beta_i)$, we have the following:

$$\Pr(n_i = r) = \binom{n}{r} \beta_i^r (1 - \beta_i)^{n-r}.$$

Then we compute the partial derivative of the probability with respect to β_i as follows:

$$\begin{aligned}
\frac{\partial \Pr(n_i = r)}{\partial \beta_i} &= \binom{n}{r} \beta_i^{r-1} (1 - \beta_i)^{n-r-1} (r(1 - \beta_i) - (n - r)\beta_i) \\
&< \binom{n}{r} \beta_i^{r-1} (1 - \beta_i)^{n-r-1} (\tau - \beta_i)n.
\end{aligned}$$

The partial derivative is smaller than 0 when $\tau < \beta_i$. Therefore, the probability $\Pr(n_i = r)$ decreases as β_i increases for any integer $r \in (n - \tau n - \underline{\alpha}_i n, \tau n)$. Thus, the lower bound of TDR_i increases as β_i becomes closer to 1.

3 Proof of Theorem 2

For $C \sim Q$, we denote $n_1 = BA(D(C), w_1)n$ and $n_j = BA(D(C), w_j)n$ for $j \in \{1, 2, \dots, s\}$. Then, we have the following:

$$\begin{aligned}
FDR &= 1 - \Pr(\max_{j \in \{1, 2, \dots, s\}} n_j < \tau n) \\
&= 1 - \Pr(n_1 < \tau n \wedge \max_{j \in \{2, 3, \dots, s\}} n_j < \tau n).
\end{aligned}$$

To derive an upper bound of FDR, we denote:

$$\begin{aligned}
|w - w_1|_1 &= n - n_1, \\
|w_1 - w_j|_1 &= n - BA(w_1, w_j)n, \\
|w - w_j|_1 &= n - n_j.
\end{aligned}$$

According to the triangle inequality, we have the following:

$$\begin{aligned}
|w - w_j|_1 &\geq |w_1 - w_j|_1 - |w - w_1|_1 \\
&= n_1 - BA(w_1, w_j)n.
\end{aligned}$$

Therefore, we derive the upper bound of n_j for $j \in \{2, 3, \dots, s\}$ as follows:

$$\begin{aligned}
n_j &= n - |w - w_j|_1 \\
&\leq n - n_1 + BA(w_1, w_j)n.
\end{aligned}$$

Thus, we derive the upper bound of FDR as follows:

$$\begin{aligned}
FDR &= 1 - \Pr(n_1 < \tau n \wedge \max_{j \in \{2, 3, \dots, s\}} n_j < \tau n) \\
&\leq 1 - \Pr(n_1 < \tau n \wedge \max_{j \in \{2, 3, \dots, s\}} n - n_1 + BA(w_1, w_j)n < \tau n) \\
&= 1 - \Pr(n_1 < \tau n \wedge n - n_1 + \bar{\alpha}_1 n < \tau n) \\
&= 1 - \Pr(n - \tau n + \bar{\alpha}_1 n < n_1 < \tau n) \\
&= \Pr(n_1 \geq \tau n) + \Pr(n_1 \leq n - \tau n + \bar{\alpha}_1 n),
\end{aligned}$$

where $n_1 \sim B(n, 0.5)$ and $\bar{\alpha}_1 = \max_{j \in \{2, 3, \dots, s\}} BA(w_1, w_j)$.

.4 Proof of Theorem 3

For $C \sim Q$, we denote $n_j = BA(D(C), w_j)n$ for $j \in \{1, 2, \dots, s\}$, and we have the following:

$$\begin{aligned} FDR &= 1 - \Pr\left(\max_{j \in \{1, 2, \dots, s\}} n_j < \tau n\right) \\ &= 1 - \prod_{j \in \{1, 2, \dots, s\}} \Pr(n_j < \tau n). \end{aligned}$$

According to Definition 4, for any $k \in \{1, 2, \dots, n\}$ and any $j \in \{1, 2, \dots, s\}$, the decoding of each bit is independent and the probability that $D(C)[k]$ matches with $w_j[k]$ is at most $0.5 + \gamma$ no matter $w_j[k]$ is 1 or 0. Therefore, we have the following:

$$\begin{aligned} FDR &= 1 - \prod_{j \in \{1, 2, \dots, s\}} \Pr(n_j < \tau n) \\ &\leq 1 - \Pr(n' < \tau n)^s, \end{aligned}$$

where n' follows the binomial distribution with parameters n and $0.5 + \gamma$, i.e., $n' \sim B(n, 0.5 + \gamma)$.

.5 Proof of Corollary 2

According to Theorem 3, the probability $\Pr(n' < \tau n)$ increases when γ decreases. Therefore, the upper bound of FDR decreases as γ becomes closer to 0.

.6 Proof of Theorem 4

For $C \sim \mathcal{P}_i$, we denote $w = D(C)$, $n_i = BA(w, w_i)n$, and $n_j = BA(w, w_j)n$ for $j \in \{1, 2, \dots, s\}$. Then we have the following:

$$\begin{aligned} |w - \neg w_i|_1 &= n_i, \\ |\neg w_i - w_j|_1 &= BA(w_i, w_j)n, \\ |w - w_j|_1 &= n - n_j. \end{aligned}$$

According to the triangle inequality, we have:

$$\begin{aligned} |w - w_j|_1 &\geq |w - \neg w_i|_1 - |\neg w_i - w_j|_1 \\ &= n_i - BA(w_i, w_j)n. \end{aligned}$$

Therefore, we derive the upper bound of n_j for $j \in \{1, 2, \dots, s\}/\{i\}$ as follows:

$$\begin{aligned} n_j &= n - |w - w_j|_1 \\ &\leq n - n_i + BA(w_i, w_j)n. \end{aligned}$$

Thus, we derive the lower bound of TAR_i as follows:

$$\begin{aligned} TAR_i &= \Pr\left(\max_{j \in \{1, 2, \dots, s\}} n_j \geq \tau n \wedge n_i > \max_{j \in \{1, 2, \dots, s\}/\{i\}} n_j\right) \\ &\geq \Pr\left(\max_{j \in \{1, 2, \dots, s\}} n_j \geq \tau n \wedge n_i > \max_{j \in \{1, 2, \dots, s\}/\{i\}} n - n_i + BA(w_i, w_j)n\right) \\ &= \Pr\left(\max_{j \in \{1, 2, \dots, s\}} n_j \geq \tau n \wedge n_i > \frac{n + \bar{\alpha}_i n}{2}\right) \\ &= \Pr\left(\max_{j \in \{1, 2, \dots, s\}} n_j \geq \tau n \wedge n_i > \frac{n + \bar{\alpha}_i n}{2} \mid n_i \geq \tau n\right) \cdot \Pr(n_i \geq \tau n) \\ &\quad + \Pr\left(\max_{j \in \{1, 2, \dots, s\}} n_j \geq \tau n \wedge n_i > \frac{n + \bar{\alpha}_i n}{2} \mid n_i < \tau n\right) \cdot \Pr(n_i < \tau n) \\ &\geq \Pr\left(n_i > \frac{n + \bar{\alpha}_i n}{2} \mid n_i \geq \tau n\right) \cdot \Pr(n_i \geq \tau n) \\ &= \Pr\left(n_i > \frac{n + \bar{\alpha}_i n}{2} \wedge n_i \geq \tau n\right) \\ &= \Pr\left(n_i \geq \max\left\{\lfloor \frac{1 + \bar{\alpha}_i}{2} n \rfloor + 1, \tau n\right\}\right), \end{aligned}$$

where $n_i \sim B(n, \beta_i)$ and $\bar{\alpha}_i = \max_{j \in \{1, 2, \dots, s\}/\{i\}} BA(w_i, w_j)$.

Table 5: Default parameter settings for training AWT.

Phase	Standard Training	Fine-Tuning
Optimizer	Adam	
# epochs	200	10
Batch size	16	
Learning rate	3×10^{-5}	
# warm-up iterations	6000	1000
Length of text	250	250 ± 16
Generation weight	1.5	1
Message weight	10000	
Reconstruction weight	1.5	2

Algorithm 1 $BSTA(w_s, d, m)$ **Input:** Initial watermark w_s , recursion depth d , and m .**Output:** w_s or *NotExist*.

```

1: if  $d < 0$  then
2:   return NotExist
3:  $i^* \leftarrow \arg \max_{i \in \{1, 2, \dots, s-1\}} BA(w_i, w_s)$ 
4: if  $BA(w_{i^*}, w_s) > (m + d)/n$  then
5:   return NotExist
6: else if  $BA(w_{i^*}, w_s) \leq m/n$  then
7:   return  $w_s$ 
8:  $B \leftarrow \{k | w_s[k] = w_{i^*}[k], k = 1, 2, \dots, n\}$ 
9: Choose any  $B' \subset B$  with  $|B'| = m + 1$ 
10: for all  $k \in B'$  do
11:    $w'_s \leftarrow w_s$ 
12:    $w'_s[k] \leftarrow \neg w'_s[k]$ 
13:    $w'_s \leftarrow BSTA(w'_s, d - 1, m)$ 
14:   if  $w'_s$  is not NotExist then
15:     return  $w'_s$ 
16: return NotExist

```

.7 Adversarial Training of AWT

In adversarial training, we employ T5-based paraphraser to post-process the watermarked texts generated by AWT. Due to the non-differentiable nature of the paraphrasing process, we cannot jointly adversarially train the encoder and decoder since the gradients cannot back-propagate to the encoder. To address the challenge, we first use the standard training to train AWT encoder and decoder. Then, we use the encoder to generate watermarked texts, paraphrase them, and use the paraphrased watermarked texts to fine-tune the decoder. The detail parameter settings of fine-tuning are shown in Table 5.

Algorithm 2 $NRG(w_s, m)$

Input: Initial watermark w_s and m .

Output: w_s or *NotExist*.

```
1:  $F \leftarrow \emptyset$ 
2:  $d \leftarrow m$ 
3: while  $d > 0$  do
4:    $i^* \leftarrow \arg \max_{i \in \{1, 2, \dots, s-1\}} BA(w_i, w_s)$ 
5:   if  $BA(w_{i^*}, w_s) > 2m/n$  then
6:     return NotExist
7:   else if  $BA(w_{i^*}, w_s) \leq m/n$  then
8:     return  $w_s$ 
9:    $B \leftarrow \{k | w_s[k] = w_{i^*}[k] \wedge k \notin F, k = 1, 2, \dots, n\}$ 
10:   $l \leftarrow n \cdot BA(w_{i^*}, w_s) - m$ 
11:  Sample  $B' \subset B$  with  $|B'| = l$  uniformly at random
12:  for all  $k \in B'$  do
13:     $w_s[k] \leftarrow \neg w_s[k]$ 
14:   $d \leftarrow d - l$ 
15:   $F \leftarrow F \cup B'$ 
16: return NotExist
```

Algorithm 3 Solving our watermark selection problem

Input: Existing $s - 1$ watermarks w_1, w_2, \dots, w_{s-1} .

Output: Watermark w_s .

```
1:  $m \leftarrow \max_{i \in \{1, 2, \dots, s-2\}} n \cdot BA(w_i, w_{s-1})$ 
2: while  $w_s$  is NotExist do
3:   if BSTA then
4:      $w_s \leftarrow \neg w_1$ 
5:      $w_s \leftarrow \text{BSTA}(w_s, m, m)$ 
6:   if NRG then
7:      $w_s \leftarrow \neg w_1$ 
8:      $w_s \leftarrow \text{NRG}(w_s, m)$ 
9:   if A-BSTA then
10:     $w_s \leftarrow$  sampled uniformly at random
11:     $w_s \leftarrow \text{BSTA}(w_s, d, m)$ 
12:   if  $w_s$  is NotExist then
13:      $m \leftarrow m + 1$ 
14: return  $w_s$ 
```
